

Study of thermal properties of the aluminum EN AW 2024-T3 alloy

Dragan Manasijević^{1*}, Ljubiša Balanović¹, Nebojša Tadić², Žarko Radović²,
Uroš Stamenković¹, Milan Gorgievski¹, Ivana Marković¹

¹University of Belgrade, Technical Faculty in Bor, VJ12, 19210 Bor, Serbia

²University of Montenegro, Faculty of Metallurgy and Technology, Cetinjski put, bb, 81000, Podgorica, Montenegro

Received 2 February 2024, received in revised form 20 February 2024, accepted 22 February 2024

Abstract

The thermal properties of the aluminum EN AW-2024 alloy (duralumin) delivered in the T3 condition (solution annealed, quenched, cold-deformed, and naturally aged) were experimentally investigated using differential thermal analysis (DTA), differential scanning calorimetry (DSC), and light flash apparatus (LFA) for thermal diffusivity and thermal conductivity evaluation. The microstructure of the alloy in the initial state and after heating to 400 °C was investigated by scanning electron microscope (SEM) and energy-dispersive spectroscopy. The presence of an exothermic thermal effect in the temperature range from 230 to 283 °C during the first heating of the examined sample was determined by the results of DTA/DSC analysis. The thermal diffusivity of the investigated alloy was measured in the temperature range from 25 to 400 °C using three heating runs. During the first heating, the thermal diffusivity of the investigated alloy increased with an increase in temperature up to approximately 300 °C, after which it decreased. During the second and third heating, it was observed that the measured thermal diffusivity values at temperatures lower than 300 °C were significantly higher than during the first heating, and the thermal diffusivity gradually decreased with increasing temperature in the entire investigated temperature range. Experimentally determined thermal diffusivity and density, as well as calculated specific heat capacity data, were used to determine the thermal conductivity of the studied alloy in the temperature interval from 25 to 400 °C. The obtained results indicate that initial heating to a temperature above 300 °C causes a significant increase in the values of the thermal diffusivity and thermal conductivity of the investigated 2024-T3 alloy.

Key words: 2024-T3 alloy, microstructure, DSC, thermal conductivity

1. Introduction

Duralumin is a trade name for Al-Cu(-Mg-Mn) alloys discovered in 1906 by Alfred Wilm [1, 2]. He developed the first duralumins, i.e. aluminum-based alloys with 3 to 4.5 % of copper, 0.4 to 10 % of magnesium, up to 0.7 % of manganese, 0.3 to 0.6 % of silicon, and 0.4 to 1.0 % of iron [3]. Nowadays, according to the International Alloy Designation System (IADS) developed by the Aluminum Association, these alloys belong to the 2xxx series of aluminum alloys (numerical designation with 4 numbers) [4, 5].

Alloys from the 2xxx series have a good combination of different required properties: high mecha-

nical properties as well as strength-to-weight ratio, good formability, machinability, fatigue, and acceptable damage tolerance [5–8]. Their good mechanical properties can be achieved using thermal or thermomechanical treatments, which include precipitation hardening (aging). The thermal treatments consist of heating near solvus temperature in the single-phase region to create a homogeneous solid solution, quenching to produce a supersaturated alloy, and aging during which the coherent precipitates responsible for strengthening are formed from a supersaturated solid solution [7, 9, 10]. Aging can be implemented at room temperature for several days (natural aging – T3 and T4 tempers) or at temperatures from 150 °C to 200 °C

*Corresponding author: e-mail address: dmanasijevic@tfbor.bg.ac.rs

Table 1. Chemical composition of the EN AW 2024 alloy

Component	Cu	Mg	Mn	Si	Fe	Zn	Cr	Ti	Bi	Ni
Concentration mass%	4.8	1.41	0.42	0.13	0.28	0.07	≤ 0.01	0.015	0.012	0.02

up to tens of hours (artificial aging – T6 and T8 tempers) [7].

EN AW 2024 alloy is one of the most used from 2xxx series aluminum alloys [11]. It is widely applied in the aeronautical field (aircraft fuselages, wings, rivets, etc.), architecture, railway transportation, [12], automotive industry [13], as a drill pipe material [14], etc., due to its lightweight, good strength, toughness, and crack propagation, tolerance to elastic/plastic stretching [15, 16].

Its equilibrium microstructure consists of primary α -Al dendrites with precipitates of S(Al_2CuMg) and θ (Al_2Cu) phases [15]. These stable phases are incoherent and have high interfacial energy with the matrix so their nucleation requests high driving force. Therefore, it is kinetically more suitable to nucleate coherent metastable phases firstly, which have a lower nucleation barrier [2]. According to the literature, the precipitation of the main strengthening phases during aging goes through the following paths [17]: (i) from supersaturated solid solution Guinier-Preston-Bagaryatsky (GPB) zones firstly precipitate; then S'' metastable phase (fully coherent with the matrix) occurs; whereupon the S' metastable phase (semi-coherent with the matrix) precipitates; finally at the end of precipitation sequence S(Al_2CuMg) equilibrium phase precipitates [18]; (ii) similarly, from supersaturated solid solution Guinier-Preston (GP) zones firstly precipitate, then θ'' metastable phase precipitates, after which the θ' metastable phase occurs, finally at the end of precipitation sequence the θ (Al_2Cu) equilibrium phase forms [19].

Some other phases can be found depending on the alloy composition (primarily Cu content and Cu/Mg ratio) and thermal treatment parameters [17]. Starke and Staley [20] confirmed the existence of intermetallic particles of AlCuFe and AlFeMnSi phases in addition to the standard S and θ phases.

EN AW 2024 alloy was examined from the aspect of precipitation behavior during different aging regimes in numerous papers. Sun et al. combined modification with Sr and strengthening during artificial aging. They showed that Sr refines the precipitates improving the strengthening [14]. Akande et al. [21] investigated the influence of different quenching media on the mechanical properties of the artificially aged alloy. Quenching in water gave higher ductility and hardness values than quenching in air and oil. The effect of solid-solution treatment on the microstructure and formability of the 2024 alloy was studied by Lin et al. [22]. Alexopoulos et al. [19] investigated the effect

of different artificial aging conditions on precipitation and cold deformation behavior.

The impact of deformation on the phases' precipitation was investigated by Guía-Tello et al. [5]. Also, Lin et al. confirmed that external stress accelerated the age hardening in 2024-T3 alloy by easily growing up precipitates of the S phase [23]. The influence of post-ECAP aging on the homogeneity of the 2024 alloy was investigated by Kotan et al. [24]. ECAP decreased the aging time. Double-peak age strengthening in cold-worked 2024 alloy was shown in the paper of Zhao et al. [18]. The first strengthening peak after aging for 120 min is achieved due to the precipitation of fine S' precipitates, and the second one after aging for 720 min is attributed to the particle precipitation of θ phase.

The main purpose of the investigation of Liang et al. [25] was to study the effect of solution temperature and holding time on the mechanical properties of the naturally aged alloy. Pre-aging as a potential treatment for inhibiting secondary natural aging was studied by Österreicher et al. [26].

As can be seen, the influence of aging parameters on the mechanical properties of EN AW 2024 alloys has been studied intensively. The changes in thermal properties were rarely reported [6]. However, aluminum alloys are often considered as heat sink materials to dissipate the heat away from the components, ensuring their regular operation. This helps to increase the lifespan of the components and improve the overall performance. For this type of application of aluminum alloys, knowledge of thermal properties is of key importance. For this reason, specific heat, thermal diffusivity, and thermal conductivity of EN AW 2024 alloy in the T3 temper are the focus of this research. T3 temper includes the solid solution treatment at 495°C, followed by cold rolling and natural aging.

2. Materials and methods

2.1. Materials

The as-delivered EN AW 2024-T3 alloy was in the form of sheets. The chemical composition (mass%) of the EN AW 2024 alloy is shown in Table 1.

The EN AW 2024-T3 is a medium to high-strength alloy that was solution heat-treated at 495°C, cold worked, and naturally aged to a substantially stable condition.

2.2. Microstructure analysis

The microstructural analysis of the EN AW 2024-T3 alloy was performed in the initial (as-received) state and after heating the sample from room temperature to 400 °C. The test sample was the same as for the thermal diffusivity measurements (round disk shape with 12.7 mm in diameter and 3 mm thick, with two ground plane parallel end-faces). A scanning electron microscope (VEGA 3LMU, Tescan, Czech Republic) with the energy-dispersive spectrometer (X-act, Oxford Instruments, UK) was used to analyze the microstructure. SEM-EDS analysis was performed with an accelerating voltage of 20 kV.

2.3. Thermal analysis

A simultaneous thermal analyzer (SDT Q600, TA Instruments, USA) was employed to measure the phase change temperatures of the investigated sample. The DTA/DSC device was calibrated for cell constant, temperature, and heat flow. The temperature range of the DTA/DSC investigation was 30–450 °C. The measurements were carried out using alumina crucibles under the protection of a constant stream of argon gas with a flow rate of 50 ml min⁻¹. The mass of the investigated sample was about 20 mg, while the heating rate was 10 °C min⁻¹.

2.4. Light flash apparatus (LFA)

The thermal diffusivity was determined using a low-temperature light flash apparatus (Discovery Xenon Flash DXF-500, TA Instruments, USA). In this method, the bottom surface of a plane-parallel sample is heated by a short energy pulse generated by a xenon lamp, and the resulting temperature rise on the top surface of the sample is measured using an infrared detector [27]. From the resulting temperature change of the rear face, the thermal diffusivity is calculated. The temperature range of the LFA investigation was 25–400 °C. The following temperatures were selected (for the first and following heating): 25, 50, 100, 200, 300, and 400 °C. At each temperature three measurements of the thermal diffusivity were done to allow an average result to be calculated.

Thermal diffusivity measurements were performed on the sample of the as-received alloy, which was already in T3 condition (solution annealed, quenched, cold-deformed, and naturally aged to a substantially stable condition). The first set of thermal diffusivity values was obtained during the initial heating of the sample from room temperature to 400 °C (first heating). After cooling the sample to room temperature, the thermal diffusivity was measured again by reheating the sample to 400 °C (second heating). This experimental procedure (cooling and re-

heating of the sample to 400 °C) was repeated for a third time (third heating). In this way, three sets of thermal diffusivity values were obtained in the temperature range from 25 to 400 °C, corresponding to the first, second, and third heating of the alloy.

2.5. Density measurement

The indirect Archimedean method [28] was applied to determine the density of the EN AW 2024-T3 alloy at room temperature. The density was measured using a Mettler Toledo electronic instrument.

2.6. Electrical conductivity measurements

Electrical conductivity was measured using the Forsterer SIGMATEST 2.069 eddy current conductivity meter. Electrical conductivity measurements are based on the complex impedance of the measuring probe. The technique includes nulling an absolute probe in air and placing the probe in contact with the sample surface. For nonmagnetic materials, the change in the impedance of the coil can be correlated directly to the conductivity of the material. Before each measurement, the conductivity tester was calibrated with two standard plates with an electrical conductivity of 4.362 MS m⁻¹ (7.521/a %IACS) and 58.18 MS m⁻¹ (100.3 %IACS). Electrical conductivity measurements at room temperature for samples in the as-delivered state and after the first heating cycle were performed at five measurement points, and average values of electrical conductivity were then calculated.

2.7. Thermodynamic calculation of specific heat capacity

The specific heat capacity of the investigated EN AW 2024-T3 alloy in the temperature interval 25–400 °C was calculated using the CALPHAD method [29], Pandat software, and related thermodynamic database for the multi-component aluminum-rich casting and wrought alloys [30]. By minimizing the total Gibbs energy, the thermodynamic equilibrium of the system is calculated. Several models are developed to describe the Gibbs energy of a specific phase using thermodynamic parameters. Optimization of parameters is performed so that the model fits the available experimental data for the given phase. After entering the thermodynamic models of all phases together with the optimized parameters into the program, the thermodynamic quantities and phase equilibria are calculated. All the other thermodynamic functions (specific heat capacity, enthalpy, entropy, etc.) are determined from Gibbs energy and its partial derivatives. In the case of heat capacity, it

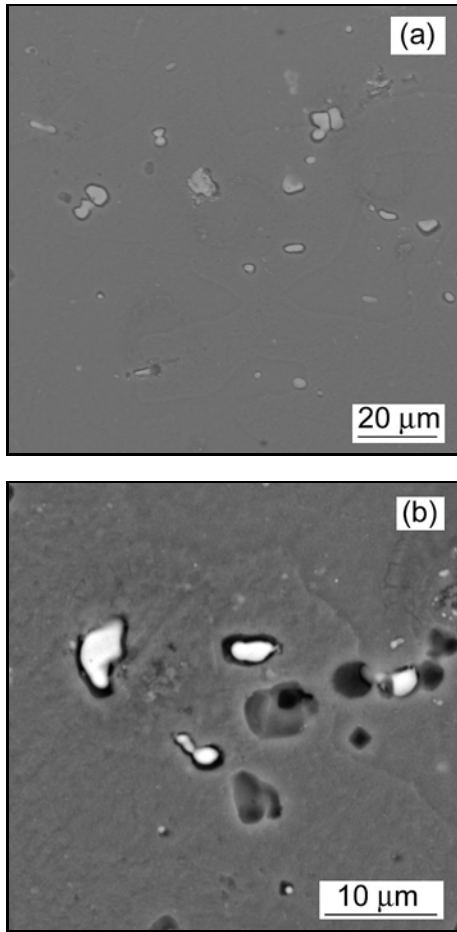


Fig. 1. SEM image of the EN AW 2024-T3 alloy in the initial state, magnification: (a) 2000× and (b) 5000×.

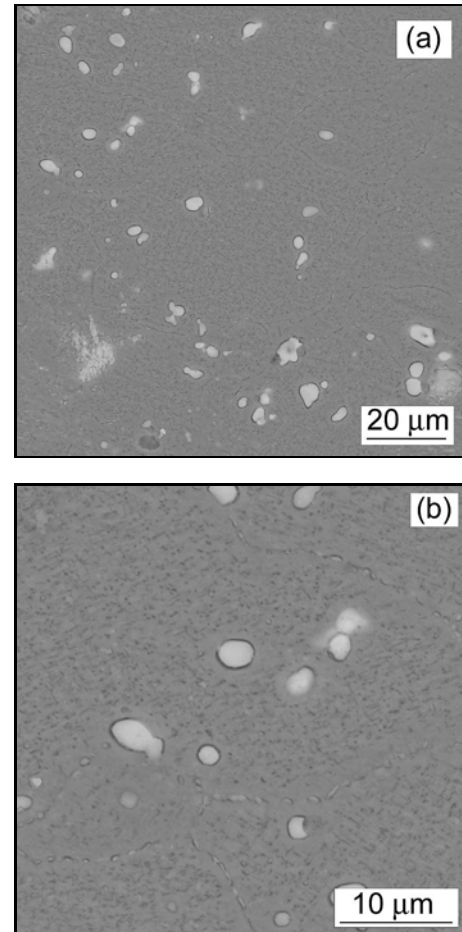


Fig. 2. SEM image of the EN AW 2024-T3 alloy after heating to 400 °C, magnification: (a) 2000× and (b) 5000×.

follows:

$$C_p = -T \frac{\partial^2 G}{\partial T^2} = \frac{\partial H}{\partial T}, \quad (1)$$

where C_p represents heat capacity, G is Gibbs energy, H is enthalpy, and T is absolute temperature.

3. Results and discussion

3.1. Microstructure investigation

The microstructure of the studied EN AW 2024-T3 alloy in the initial state and after heating to 400 °C is shown in Figs. 1 and 2.

The presence of insoluble precipitates of the θ -Al₂Cu equilibrium phase was confirmed by the results of EDS analysis. They are visible in the microstructure as bright, relatively large particles located inside the grains of the aluminum solid solution – α phase. They are present in the microstructure

of the alloy in the initial state (Figs. 1a,b) and after heating (Figs. 2a,b). These precipitates were formed during solidification of the alloy. They remained undissolved during the heat treatment of the alloy and did not contribute to its strengthening.

The microstructure of the EN AW 2024-T3 alloy after heating to 400 °C is characterized by the presence of submicronic particles (dispersoids) homogeneously distributed throughout the aluminum matrix. The small precipitates along the grain boundaries of aluminum solid solution are also visible. According to the results of EDS analysis, these precipitates correspond to the S-Al₂CuMg phase.

3.2. Investigation of thermal behavior

DTA/DSC techniques were used to study phase transition temperatures during the heating of the EN AW 2024-T3 alloy. The DTA heating curve for the first heating run is shown in Fig. 3. The presence of one broad exothermic peak was identified in the temperature range from 230 to 283 °C. The second and

Table 2. Density, thermal diffusivity, specific heat capacity, and thermal conductivity of the investigated EN AW 2024-T3 alloy in the temperature range 25–400 °C

Temperature (°C)	Density (g cm ⁻³)	Specific heat capacity (J g ⁻¹ K ⁻¹)	Thermal diffusivity (mm ² s ⁻¹)		Thermal conductivity (W m ⁻¹ K ⁻¹)	
			first heating	second heating	first heating	second heating
25	2.77	0.877	49.86	71.37	121.1	173.4
50	2.76	0.892	50.85	69.59	125.2	171.3
100	2.75	0.918	52.68	69.19	133.0	174.7
200	2.73	0.962	56.48	68.74	148.3	180.5
300	2.71	1.003	65.48	67.33	178.0	183.0
400	2.69	1.044	62.78	63.43	176.3	178.1

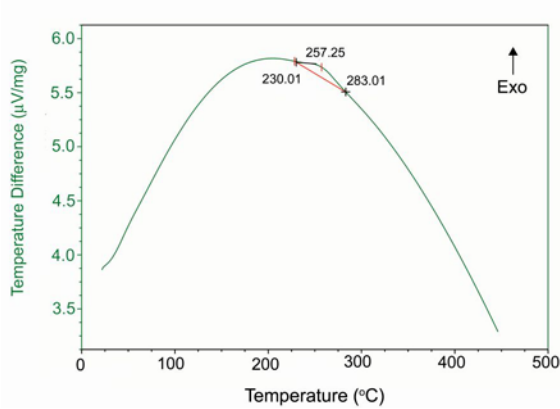


Fig. 3. DTA curve of studied EN AW 2024-T3 sample in the first heating run.

subsequent heating runs did not identify any exothermic or endothermic phase transitions.

The exothermic heat effect during the initial heating of the studied alloy indicates the precipitation process, which is characterized by the release of heat. In commercial EN AW 2024 alloy precipitation sequence includes the formation of Guinier-Preston-Bagaryatsky (GPB) zones followed by precipitation of S'' and S' metastable phases before the precipitation of stable S-Al₂CuMg phase [17, 31]. According to the results of Zmywaczyk et al. [6] and Semnani and Degischer [32], the exothermic heat effect in the temperature range identified in the present study is related to the precipitation of S' and S phases. This is also in accordance with the results of the microstructural analysis.

3.3. Investigation of thermal properties

The obtained density value for the EN AW 2024-T3 alloy is 2.77 g cm⁻³. Based on the density measurement for pure Al, the measurement uncertainty was assessed to be ± 1%. The change in density with temperature in the studied temperature range was de-

termined based on the coefficient of linear expansion proposed by Hidnet and Krider [33] for aluminum alloys with low copper content.

Next, thermal diffusivity was directly measured in the temperature interval 25–400 °C using the light flash method. The thermal diffusivity values obtained during the first and second heating are given in Table 2.

The specific heat capacity of the investigated EN AW 2024-T3 alloy in the temperature interval 25–400 °C was calculated using the CALPHAD method [29].

Finally, the thermal conductivity of the alloys was calculated using values of thermal diffusivity, density, and specific heat capacity following the fundamental equation, Eq. (2):

$$\lambda = \alpha \rho C_p, \quad (2)$$

where λ represents thermal conductivity (W m⁻¹ K⁻¹), α is thermal diffusivity (m² s⁻¹), ρ is the value of density (kg m⁻³), and C_p is the specific heat capacity (J g⁻¹ K⁻¹) of the studied alloy.

The obtained results are shown in Table 2.

Figure 4 shows temperature dependences of thermal diffusivity for the EN AW 2024-T3 alloy obtained from the first and subsequent heating runs. Bearing in mind the standard deviation of experimental points and errors from instrument measurement, the uncertainty in thermal diffusivity measurements was estimated to be about ± 3%.

During the first heating, the thermal diffusivity of the investigated alloy increased with the increase in temperature up to approximately 300 °C, after which it decreased. The measured thermal diffusivity values obtained during the second and third heating runs were nearly identical. This means that, after the first heating, the microstructure of the alloy remained fairly unchanged during subsequent heating runs. During the second and third heating, the measured thermal diffusivity values at temperatures lower than 300 °C were significantly higher than during the

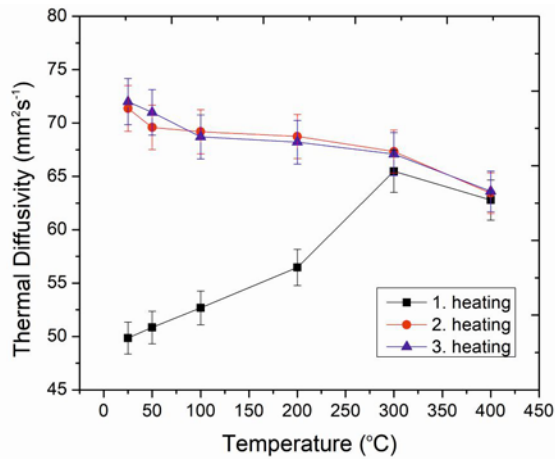


Fig. 4. Thermal diffusivity as a function of temperature for the EN AW 2024-T3 alloy obtained from the first and subsequent heating runs.

first heating, and the thermal diffusivity gradually decreased with increasing temperature in the entire investigated temperature range. The significant increase in thermal diffusivity below 300 °C after the first heating is the result of artificial aging, i.e. formation of precipitates of S' and S intermetallic compounds. This is in line with the results of microstructural analysis and DTA measurements. Thermal diffusivity dependence on temperature changed in the following heating cycles. Considering that the microstructure of the alloy remained the same during subsequent heating cycles, the decrease in thermal conductivity with an increase in temperature can be attributed to the increased lattice vibrations caused by the higher thermal energy. As temperature increases, the atoms in the metal lattice vibrate more vigorously, which leads to greater scattering of the electrons that carry heat. This increased scattering reduces the mean free path of the electrons, thereby decreasing the overall thermal diffusivity of the alloy.

The specific heat capacity dependence on temperature for the EN AW 2024-T3 alloy is shown in Fig. 5.

The specific heat capacity of the investigated EN AW 2024-T3 alloy steadily increases with increasing temperature from $0.877 \text{ J g}^{-1} \text{ K}^{-1}$ at 25 °C to $1.044 \text{ J g}^{-1} \text{ K}^{-1}$ at 400 °C.

The thermal conductivities of the investigated alloy were calculated based on the measured values of thermal diffusivity during the first and second heating, the measured density of the alloy, and the calculated specific heat capacity data. The obtained temperature dependences of thermal conductivity for the EN AW 2024-T3 alloy in the studied temperature interval are presented in Fig. 6.

Similar to the case of thermal diffusivity, the obtained values of thermal conductivity during the initial heating of the alloy at temperatures below 300 °C

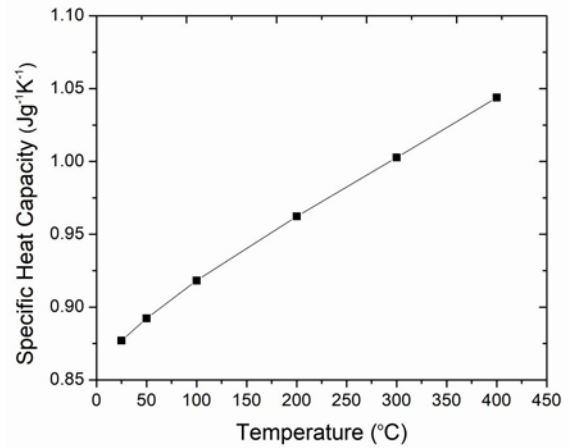


Fig. 5. Specific heat capacity of the EN AW 2024-T3 alloy as a function of temperature.

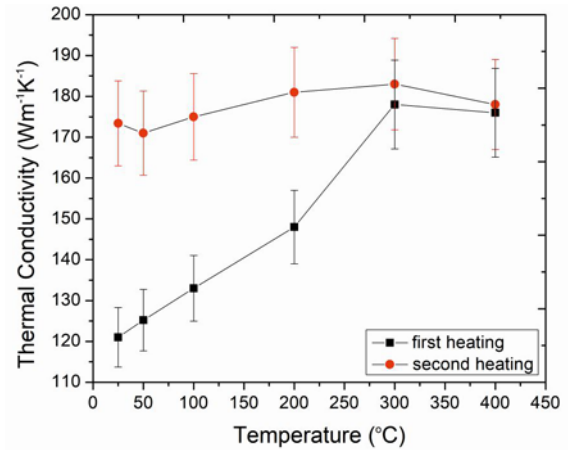


Fig. 6. Thermal conductivities of the studied EN AW 2024-T3 alloy based on the thermal diffusivity values obtained during first and second heating.

were significantly lower than the corresponding values obtained during the second heating.

Based on thermal diffusivity data from the first heating, the obtained value of thermal conductivity at 25 °C was $121.1 \text{ W m}^{-1} \text{ K}^{-1}$. This result is in excellent agreement with the literature value of thermal conductivity for the EN AW 2024-T3 alloy ($121.0 \text{ W m}^{-1} \text{ K}^{-1}$) [34].

Thermal conductivities of the studied EN AW 2024-T3 alloy at room temperature in the as-delivered state and after the first heating cycle were also estimated using the Wiedemann-Franz law and measured values of electrical conductivity.

The thermal conductivity of metallic materials is composed of electronic thermal conductivity λ_e and phononic (or lattice) thermal conductivity λ_p [35]:

$$\lambda = \lambda_e + \lambda_p. \quad (3)$$

The Wiedemann-Franz law gives the relationship between electronic thermal conductivity λ_e , electrical conductivity σ , and temperature T [35]:

$$\frac{\lambda_e}{\sigma} = L_0 T. \quad (4)$$

Hatch et al. [36] proposed that the Lorentz constant L_0 of aluminum alloys is $2.1 \times 10^{-8} \text{ W } \Omega \text{ K}^{-2}$, and c is $12.6 \text{ W m}^{-1} \text{ K}^{-1}$. Thus, the following equation can be used for the prediction of total thermal conductivity for aluminum alloys:

$$\lambda = \sigma L_0 T + c. \quad (5)$$

Using the measured values of electrical conductivity (average value 15.5 MS m^{-1} for the as-delivered state and 23.5 MS m^{-1} after the first heating cycle) and Eq. (5), it follows that the predicted thermal conductivities of the investigated alloy in the as-delivered condition and after the first heating cycle are 109.6 and $159.7 \text{ W m}^{-1} \text{ K}^{-1}$. The calculated values are comparable with the experimentally obtained values of thermal conductivity (121.1 and $173.4 \text{ W m}^{-1} \text{ K}^{-1}$).

It is known that the weakening effect of alloying elements in the solid solution state on the thermal conductivity of aluminum is much more significant than when in the precipitated state [37]. The added solute atoms induce the lattice distortion which leads to an increase in electron scattering and a decrease in the thermal conductivity of alloy. On the other hand, precipitation of solute atoms can weaken the lattice distortion by reducing the supersaturation of the Al matrix, which is beneficial to thermal conductivity. It is also established that the level of influence of different alloying elements in solid solution on lowering the thermal conductivity of aluminum is not the same and that it is related to the variation of outer electronic structure and atom radii difference between alloying elements and aluminum [37]. Common alloying elements such as Si, Cu, Mg, and Zn show more similar outer electronic structures to aluminum than trace alloying elements (Cr, V, Mn, Ti). Therefore, the influence of common alloying elements on the reduction of thermal conductivity in aluminum alloys is significantly weaker than in the case of trace alloying elements. For this reason, it is necessary to strictly control the content of trace elements in aluminum alloys for industrial heat dissipation components [37].

Thus, it can be concluded that the increase in thermal conductivity of the investigated alloy after initial heating is caused by the formation of precipitates from supersaturated aluminum solid solution.

4. Conclusions

In this study, the microstructure and thermal properties of the EN AW 2024-T3 alloy in the as-delivered state and after heating to 400°C were examined. The following conclusions can be derived:

(a) The microstructure analysis confirmed the presence of intermetallic precipitates corresponding to the equilibrium $\theta\text{-Al}_2\text{Cu}$ phase in both initial and after-heating conditions. Heating the alloy up to 400°C caused the appearance of a large number of very small precipitates visible by SEM uniformly distributed within the grain and along the grain boundaries of the aluminum solid solution. Precipitates of the $\text{S-Al}_2\text{CuMg}$ phase were observed along grain boundaries.

(b) The results of DTA/DSC analysis revealed the exothermic thermal effect in the temperature range from 230 to 283°C during the heating of the alloy. According to the literature data, this thermal effect is associated with the formation of precipitates of S' and S phases during artificial aging. Succeeding heating runs did not indicate the existence of any phase transitions in the studied temperature range.

(c) The obtained density value for the EN AW 2024-T3 alloy is 2.77 g cm^{-3} at room temperature, and it continuously decreases with the increase in temperature up to 400°C to a value of 2.69 g cm^{-3} .

(d) Specific heat capacity of the investigated EN AW 2024-T3 alloy grows approximately linearly with increasing temperature from $0.877 \text{ J g}^{-1} \text{ K}^{-1}$ at 25°C to $1.044 \text{ J g}^{-1} \text{ K}^{-1}$ at 400°C .

(e) The microstructure changes caused by the first heating to 400°C had a significant effect on thermal diffusivity and thermal conductivity values obtained during subsequent heating runs. The formation of precipitates during the heating, which consumed solute elements in the aluminum matrix, contributed to the increase in thermal diffusivity and thermal conductivity of the studied EN AW 2024-T3 alloy. The obtained thermal conductivity at the start of the first heating was $121.1 \text{ W m}^{-1} \text{ K}^{-1}$ and at the start of the second heating, $173.4 \text{ W m}^{-1} \text{ K}^{-1}$.

Acknowledgements

The research presented in this paper was done with the financial support of the Ministry of Science, Technological Development and Innovations of the Republic of Serbia, with the funding of the scientific research work at the University of Belgrade, Technical Faculty in Bor, according to the contract with number 451-03-47/2023-01/200131.

References

- [1] M. Brunet, B. Malard, N. Ratel-Ramond, C. Deshayes, S. Joulié, B. Warot-Fonrose, P. Sciau, J. Douin, F. De Geuser, A. Deschamps, Precipitation in original Duralumin A-U4G versus modern 2017A alloy, *Materialia* 8 (2019) 100429. <https://doi.org/10.1016/j.mtla.2019.100429>
- [2] C. Sigli, F. De Geuser, A. Deschamps, J. Lépinoux, M. Perez, Recent advances in the metallurgy of aluminum alloys. Part II: Age hardening, *Comptes Rendus Physique* 19 (2018) 688–709. <https://doi.org/10.1016/j.crhy.2018.10.012>
- [3] G. C. Smith, Age hardening of metals, *Progress in Metal Physics* 1 (1949) 163–192. [https://doi.org/10.1016/0502-8205\(49\)90006-4](https://doi.org/10.1016/0502-8205(49)90006-4)
- [4] <https://www.aluminum.org/>
- [5] J. C. Guía-Tello, C. G. Garay-Reyes, M. A. Ruiz-Esparza-Rodríguez, L. J. García-Hernandez, J. Aguilar Santill, I. Estrada-Guel, R. Martínez-Sánchez, Effect of plastic deformation on the precipitation reaction in 2024 alloys, *Materials Chemistry and Physics* 271 (2021) 124927. <https://doi.org/10.1016/j.matchemphys.2021.124927>
- [6] J. Zmywaczyk, J. Sienkiewicz, P. Koniorczyk, J. Godzimirski, M. Zielinski, Investigation of thermophysical properties of AW-2024-T3 bare and clad aluminum alloys, *Materials* 13 (2020) 3345. <https://doi.org/10.3390/ma13153345>
- [7] A. Cochard, K. Zhu, S. Joulié, J. Douin, J. Huez, L. Robbiola, P. Sciau, M. Brunet, Natural aging on Al-Cu-Mg structural hardening alloys – Investigation of two historical duralumins for aeronautics, *Materials Science & Engineering A* 690 (2017) 259–269. <https://doi.org/10.1016/j.msea.2017.03.003>
- [8] R. Su, Y. Jia, G. Li, Y. Qu, R. Li, Effect of deformation amount on microstructure and properties of AA2024-T814 with deep cryogenic treatment, *Journal of Alloys and Compounds* 947 (2023) 169578. <https://doi.org/10.1016/j.jallcom.2023.169578>
- [9] S. P. Ringer, K. Hono, T. Saksai, I. J. Polmear, Cluster hardening in an aged Al-Cu-Mg alloy, *Scripta Materialia* 36 (1997) 517–521. [https://doi.org/10.1016/S1359-6462\(96\)00415-0](https://doi.org/10.1016/S1359-6462(96)00415-0)
- [10] A. M. Hassan, O. M. Bataineh, K. M. Abed, The effect of time and temperature on the precipitation behavior and hardness of Al–4wt.%Cu alloy using design of experiments, *Journal of Materials Processing Technology* 204 (2008) 343–349. <https://doi.org/10.1016/j.jmatprotec.2007.11.047>
- [11] A. May, M. A. Belouchrani, S. Taharboucht, A. Boudras, Influence of heat treatment on the fatigue behaviour of two aluminium alloys 2024 and 2024 plated, *Procedia Engineering* 2 (2010) 1795–1804. <https://doi.org/10.1016/j.proeng.2010.03.193>
- [12] L. Sun, Y. Guo, L. Chen, G. Zhao, Effects of solution and aging treatments on the microstructure and mechanical properties of cold rolled 2024 Al alloy sheet, *Journal of Materials Research and Technology* 12 (2021) 1126–1142. <https://doi.org/10.1016/j.jmrt.2021.03.051>
- [13] F. E. El Garchani, H. Lgaz, S. Kaya, H. S. Lee, S. M. Ibrahim, M. Chafiq, Y. G. Ko, M. R. Kabiri, Effects of heat treatment on the corrosion behavior and mechanical properties of aluminum alloy 2024, *Journal of Materials Research and Technology*, 25 (2023) 1355–1363. <https://doi.org/10.1016/j.jmrt.2023.05.278>
- [14] Z. Sun, Y. Ma, S. Ma, H. Xiong, B. Chen, Mechanical properties and corrosion resistance enhancement of 2024 aluminum alloy for drill pipe after heat treatment and Sr modification, *Materials Today Communications* 36 (2023) 106805. <https://doi.org/10.1016/j.mtcomm.2023.106805>
- [15] Y. Dong, S. Shuai, J. Yu, W. Xuan, Z. Zhang, J. Wang, Z. Ren, Effect of high static magnetic field on the microstructure and mechanical properties of directionally solidified alloy 2024, *Journal of Alloys and Compounds* 749 (2018) 978–989. <https://doi.org/10.1016/j.jallcom.2018.03.259>
- [16] A. Djili, B. Bezzazi, N. Zioui, M. Haboussi, Effect of natural aging on the tensile properties and the toughness of friction stir welds of 2024-T3 aluminum alloy, *Journal of Advanced Joining Processes* 8 (2023) 100153. <https://doi.org/10.1016/j.jajp.2023.100153>
- [17] M. Fujda, R. Mišičko, L. Rusňáková, M. Sojko, Effect of solution annealing temperature on structure and mechanical properties of EN AW 2024 aluminium alloy, *Journal of Metals, Materials and Minerals* 17 (2007) 35–40.
- [18] Y. L. Zhao, Z. Q. Yang, Z. Zhang, G. Y. Su, X. L. Ma, Double-peak age strengthening of cold-worked 2024 aluminum alloy, *Acta Materialia* 61 (2013) 1624–1638. <https://doi.org/10.1016/j.actamat.2012.11.039>
- [19] N. D. Alexopoulos, Z. Velonaki, C. I. Stergiou, S. K. Kourkoulis, Effect of ageing on precipitation kinetics, tensile and work hardening behavior of Al-Cu-Mg (2024) alloy, *Materials Science & Engineering A* 700 (2017) 457–467. <https://doi.org/10.1016/j.msea.2017.05.090>
- [20] E. A. Starke, J. T. Staley, Application of modern aluminum alloys to aircraft, *Progress in Aerospace Sciences* 32 (1996) 131–172. [https://doi.org/10.1016/0376-0421\(95\)00004-6](https://doi.org/10.1016/0376-0421(95)00004-6)
- [21] S. Akande, O. E. Ajaiyeoba, T. M. Azeza, O. M. Ikumapayi, S. A. Akinlabi, E. T. Akinlabi, Investigating the precipitation hardening of 2024 aluminium alloy under different quenching media, *Materials Today: Proceedings* 62 (2022) 4271–4274. <https://doi.org/10.1016/j.matpr.2022.04.775>
- [22] C. W. Lin, K. J. Chen, F. Y. Hung, T. S. Lui, H. P. Chen, Impact of solid-solution treatment on microstructural characteristics and formability of rotary-swaged 2024 alloy tubes, *Journal of Materials Research and Technology* 8 (2019) 3137–3148. <https://doi.org/10.1016/j.jmrt.2018.12.029>
- [23] Y. C. Lin, Y. C. Xia, Y. Q. Jiang, H. M. Zhou, L. T. Li, Precipitation hardening of 2024-T3 aluminum alloy during creep aging, *Materials Science & Engineering A* 565 (2013) 420–429. <https://doi.org/10.1016/j.msea.2012.12.058>
- [24] G. Kotan, E. Tan, Y. E. Kalay, C. H. Gur, Homogenization of ECAPed Al 2024 alloy through age-hardening, *Materials Science & Engineering A* 559 (2013) 601–606. <https://doi.org/10.1016/j.msea.2012.08.148>
- [25] M. Liang, L. Chen, G. Zhao, Y. Guo, Effects of solution treatment on the microstructure and mechanical properties of naturally aged EN AW 2024 Al alloy sheet, *Journal of Alloys and Compounds* 824 (2020)

153943.
<https://doi.org/10.1016/j.jallcom.2020.153943>
- [26] J. A. Österreicher, D. Nebeling, F. Grabner, A. Cerny, G. A. Zickler, J. Eriksson, G. Wikström, W. Suppan, C. M. Schlögl, Secondary ageing and formability of an Al-Cu-Mg alloy (2024) in W and underaged tempers, *Materials & Design* 226 (2023) 111634. <https://doi.org/10.1016/j.matdes.2023.111634>
- [27] W. J. Parker, R. J. Jenkins, C. P. Butler, G. L. Abbott, Flash method of determining thermal diffusivity, heat capacity, and thermal conductivity, *J. Appl. Phys.* 32 (1961) 1679–1684. <https://doi.org/10.1063/1.1728417>
- [28] L. Wang, A. P. Xian, Density measurement of Sn-40Pb, Sn-57Bi, and Sn-9Zn by indirect Archimedean method, *J. Electron Mater.* 34 (2005) 1414–1419. <https://doi.org/10.1007/s11664-005-0199-x>
- [29] H. L. Lukas, S. G. Fries, B. Sundman, *Computational Thermodynamics: The Calphad Method*, First edition, Cambridge University Press, Cambridge, 2007. <https://doi.org/10.1017/CBO9780511804137>
- [30] W. Cao, S. L. Chen, F. Zhang, K. Wu, Y. Yang, Y. A. Chang, R. Schmid-Fetzer, W. A. Oates, PANDAT Software with PanEngine, PanOptimizer and Pan-Precipitation for Multi-Component Phase Diagram Calculation and Materials Property Simulation, *Calphad* 33 (2009) 328–342. <https://doi.org/10.1016/j.calphad.2008.08.004>
- [31] P. Ratchev, B. Verlinden, P. De Smet, P. Van Houtte, Precipitation hardening of an Al–4.2 wt% Mg–0.6 wt% Cu alloy, *Acta Materialia* 46 (1998) 3523–3533. [https://doi.org/10.1016/S1359-6454\(98\)00033-0](https://doi.org/10.1016/S1359-6454(98)00033-0)
- [32] H. M. Semnani, H. P. Degischer, Precipitation in AlCu4.3 and AlCu4Mg alloys studied by dilatometry and calorimetry, *Kovove Materialy-Metallic Materials* 49 (2011) 369–374. https://doi.org/10.4149/km_2011_5_369
- [33] P. Hidnert, H. S. Krider, Thermal expansion of aluminum and some aluminum, *J. Res. Natl. Bur. Stand.* 48 (1952) 209. <https://doi.org/10.6028/JRES.048.030>
- [34] ASM International Handbook Committee: Properties and selection: Nonferrous alloys and special-purpose materials, 2, ASM international, Materials Park, OH, 1990. <https://doi.org/10.31399/asm.hb.v02.9781627081627>
- [35] T. M. Tritt (Ed.), *Thermal Conductivity: Theory, Properties, and Applications*, Springer Science & Business Media, 2005. <https://doi.org/10.1007/b136496>
- [36] J. E. Hatch, *Aluminum: Properties and Physical Metallurgy*, ASM international: Metals Park, OH, USA, 1984. ISBN: 978-0-87170-176-3.
- [37] A. Zhang, Y. Li, Effect of alloying elements on thermal conductivity of aluminum, *Journal of Materials Research* 38 (2023) 2049–2058. <https://doi.org/10.1557/s43578-023-00942-w>